CSCE Annual Conference

Growing with youth – Croître avec les jeunes

Laval (Greater Montreal)

June 12 - 15, 2019

PERFORMANCE OF LIGHTWEIGHT SELF-CONSOLIDATING CONCRETE COLUMNS REINFORCED WITH GFRP BARS AND SPIRALS

Sanni Bakouregui, A.[1,2] Mohamed, H. M., [1,3] Yahia, A.[1,4] Benmokrane, B.[1,5]

[1] Department of Civil Engineering, Université de Sherbrooke, Sherbrooke, Quebec, Canada.

[2] Abdoulaye.Sanni.Bakouregui@usherbrooke.ca

[3] Hamdy.Mohamed@USherbrooke.ca

[4] Ammar.Yahia@USherbrooke.ca

[5] Brahim.Benmokrane@USherbrooke.ca

Abstract: This paper presents test results of an experimental program to describe the behavior of circular lightweight self-consolidating concrete (LWSCC) columns reinforced with glass fiber-reinforced polymer (GFRP) bars and spirals. The 300 mm diameter columns were designed according to CAN/CSA S806-12 code requirements. The columns were constructed using LWSCC with compressive strength of 52 MPa and tested under axial and eccentric loading. The test parameter was the value of the applied eccentricity (0 mm, 50 mm and 200 mm). The study was conducted to investigate whether the type of concrete and the compressive and tensile behavior of longitudinal GFRP bars affect the columns performance under eccentric loading and to develop experimentally the load-moment interaction diagram. In addition, the study aimed at providing basic technical information and yielding better understanding of the eccentric behavior of circular GFRP reinforced LWSCC columns. Test results indicated that the failure process of the tested column was similar to conventional reinforced concrete columns.

1. INTRODUCTION

Structural lightweight aggregate concrete (LWAC) has benefits in reducing the weight of precast concrete elements. The weight of concrete structures is large compared with the imposed load these can carry. A relatively small reduction in weight, particularly for beams and columns, can lead to considerable savings cost construction (Comité euro-international du béton. *et al.*, 1977).The average weight reduction of lightweight concrete ranging from 25% to 35% and its structural capacity is comparable to normal weight concrete (NWC) (Harmon, 2007; Mousa *et al.*, 2018). The air-dry density of LWAC is less than 1850 kg/m^3 with a 28-day compressive strength not less than 20 MPa (CAN/CSA A23.3, 2014). LWAC is versatile material and has better fire resistance than normal weight concrete because of its lower thermal conductivity and lower coefficient of thermal expansion (ACI Committee 213, 2014). LWAC can improve the seismic resistance capacity of building structures (Rabbat *et al.*, 1986). LWAC has many and varied applications, including multi-storey building frames and floors, shell roofs, folded plates, bridges, precast elements and prestressed structures (Chandra et Berntsson, 2002; International Congress on Lightweight Concrete *et al.*, 1968). Lightweight aggregate self-compacting concrete (LWSCC) comprises a high performance material that combines the advantages of SLWAC, with self-compacting characteristics that are reflected into the material's filling and passing ability and segregation resistance (Papanicolaou et Kaffetzakis, 2011).

In recent years, the use of fiber reinforced polymer (FRP) as an alternative material has been increased. FRP materials exhibit several properties such as high strength-to-weight ratio, high stiffness-to-weight ratio, non-corrodible characteristics, high impact and fatigue resistance. FRP materials have been utilized with success in many demonstration projects across the world as internal reinforcements, external reinforcement, and for prestressing (Benmokrane *et al.*, 2007; Moy, 2013). Since FRP bars are lightweight, the use of FRP bars and structural lightweight concrete can benefit in heavy reinforced construction where the weight is problematic. Furthermore, the application of LWAC could reduce heating energy consumption by 15% compared with normal weight concrete in buildings located in European countries (Real *et al.*, 2016). Therefore, the use of LWAC with FRP bars may be suitable for durable, environment-friendly, and highly sustainable infrastructures.

Extensive research has been carried out regarding the flexural and axial performance of normal weight concrete members reinforced with FRP bars. There is a scarcity of published experimental results on the axial and flexure behavior of FRP reinforced LWAC columns. There is no experimental data concerning the use of FRP stirrups as confinement elements for concrete columns, pier columns, piles using lightweight concrete as known by the authors. This is partially due to a lack of experimental data, which can describe the behaviour of members reinforced with such materials. This study presents an experimental study aimed at investigating the performance of circular LWSCC columns reinforced with glass FRP (GFRP) bars and spirals subjected to axial and eccentric loading.

2. EXPERIMENTAL INVESTIGATION

2.1 Test Specimens

In this study, three circular RC columns were tested under axial and eccentric load. All the columns have 305 mm diameter (12'') and 1500 mm (60'') height. These dimensions were selected to ensure the specimens were large enough to be considered full-size specimens and fit in the testing machine. The reinforcements were designed according to the CAN/CSA S806-12 requirements. All the columns were reinforced with eight No. 5 (15 M) GFRP longitudinal bars, providing a longitudinal reinforcement ratio of 2.2% and with spiral No. 3 (10M) GFRP at 80 mm pitch. The pitch of the spiral at the top and bottom of the columns were reduced to 50 mm to avoid premature failure. The concrete cover of each specimen was designed with a thickness of 25 mm. Three different levels of eccentricities equal to 0 mm, 50 mm and 200 mm corresponding to eccentricity-to-diameter ratio of 0%, 16.4%, and 65.7% were considered. Table 1 shows the test matrix and specimen details. GFRP cages were assembled and were inserted into the formwork inside stiff Sonotubes as shown in Figure 1.

Table 1: Test matrix and specimen details

Specimen	e (mm)	e/D (%)	Longitudinal Bars		Transverse Spiral		
			ρ_f %	No.	ρ_{sp} %	No.	pitch (mm)
C0	0	0					
C50	50	16.4	2.2	8 No.5	0.95	3	80
C200	200	65.7					

2.2 Material Properties

FRP bars

Sand-coated No. 5 (15M) straight GFRP reinforcing bars were used as longitudinal bars and No. 3 (10M) GFRP spiral was used as transverse reinforcement. The GFRP bars were made with vinyl ester resin. The tensile properties of the longitudinal GFRP bars were determined according to test method CSA S806 (CAN/CSA S806, 2012) Annex C. The mean tensile strength and modulus of elasticity of the tested GFRP bars (No. 5) and spirals (No. 3) were 1,289 and 1,171 MPa and 54.9 and 52.5 GPa, respectively (Table 2).

Concrete

LWSCC mixture is made with a lightweight coarse and fine aggregates according to the specifications of (ASTM C330/C330M-17a, 2017) and natural normal weight sand. The maximum sizes of coarse and fine aggregates were 14 mm and 5 mm, respectively. Lightweight aggregates used in this study were expanded shale. The aggregates were pre-wetted separately before mixing with the rest of the materials to maintain a uniform water volume fraction of 0.33. The LWSCC were prepared using ternary binder containing 70% general-use cement (GU), 25% fly ash (FA), and 5% silica fume (SF) complying with ASTM C150 (ASTM C150 / C150M-18, 2019). A ready to use polycarboxylate-based high-range water-reducing agent (HRWRA) with a solid content of 40% and a specific gravity of 1.09 density was used as superplasticizer with air entraining admixture. All the column specimens were cast on the same day. The LWSCC was prepared and mixed in the structural lab of the University of Sherbrooke. The curing process was initiated immediately after the casting by covering the concrete surface with polyethylene sheets. The columns were unmolded after one day and the water-curing process was initiated for 14 days. The equilibrium density of the LWSCC was 1807 kg/m^3 and was measured according to ASTM C567/C567M, 2014. The concrete compressive strength of 52 MPa was based on the average value of tests performed on 12 concrete cylinders 150 x 300 mm on the day of testing the column specimens.

Table 2: Mechanical properties of the GFRP reinforcement

Bar Size	Diameter (mm)	Area (mm ^{2})	Elastic Tensile Modulus (GPa)	Tensile Strength (MPa)	Tensile Strain (%)
# 3	9.5	71	52.5±2.5	f_{fu} = 1171	2.30
# 5	15.9	199	54.9±2.5	f_{fu} = 1289	2.40

GFRP cages Wooden formwork

Fig. 1 - Overview of the assembled GFRP cages and formwork

2.3 Instrumentation and testing procedures

Electrical strain gauges and linear variable differential transducers (LVDTs) were used to capture the strain distributions of the concrete, GFRP bars and spiral. Two strain gauges were placed in the longitudinal bars and one strain gauge was placed in the spiral in the compression and tension side respectively as shown in figure 2. The columns were prepared for testing by levelling the top and bottom with a thin layer of high-strength cement grout to ensure a uniform load distribution of the applied load across the cross section. Two strain gauges were placed in the concrete at the mid-height of the column in the compression side for eccentric specimens C50 and C200. For concentric specimen C0, the two strain gauges were placed in opposite directions. Figure 3 shows the preparation of the columns prior testing. The test set up was consisted of rigid steel collar designed and fabricated at the structural lab at the University of Sherbrooke. The test set-up is illustrated in figure 4. The eccentric loading was applied by moving the top and the bottom roller bearing in the steel collar. The column was then placed in the steel collar. After placing the column in the testing machine, three linear potentiometers (LPOTs) were placed respectively at the ¼, ½ and ¾ of the column height in the tension side to measure the lateral displacement of the column. Three LPOTs were mounted on the right, left and front side of the column to measure the axial displacement. The column specimens were tested under a rigid FORNEY Machine with a maximum compressive capacity of 6000 kN. The loading rate was ranged between 0.25 to 1.5 kN/s during the test by manually control the hydraulic pump. The FORNEY Machine load, the strains and the displacement were recorded using Data Acquisition System.

One strain gauge in the spiral Two strain gauges in the longitudinal bars

Fig. 2: Instrumentation of the bars and spiral

Levelling and capping Installing strain gauges in the concrete Installing steel end-cap

Fig. 3 – Specimens preparation

Fig. 4 – Test set-up

3. EXPERIMENTAL RESULTS AND DISCUSSION

3.1 CRACKING PATTERN AND FAILURE MODES

Table 3 summarizes the results of the experimental study including identification of the specimens, eccentricity, ratio eccentric over diameter, cylinder compressive strength, peak load during the test, mid-height lateral displacement at the peak load, and bending moment at the peak load. The bending moment was calculated based on Equation 1.

$$M_n = P_n(e + x_{mid}) \qquad (1)$$

Where e is the applied eccentricity, P_n is the peak load, x_{mid} is the mid-height lateral displacement at the peak load, M_n is the bending moment at the peak load.

Table 3 - Summary of test results

Specimen	e (mm)	e/D (%)	Cylinder compressive Strength f'_c (MPa)	P_n (kN)	x_{mid} (mm)	M_n (kN.m)
C0	0	0	52	3531	-	-
C50	50	16.4		1905	2.935	100.8
C200	200	65.7		439	12.995	93.5

D: diameter of the column

The behaviour of the specimens during the test and the observed failure modes are described below.

3.1.1 Specimen C0

During the ascending part of loading of the column C0 subjected to concentric load, confinement had little effect, and the concrete cover was visually free of cracks up to the first crack (95% of the peak load). The failure pattern began with the appearance of horizontal tensile crack at mid-height of the column. Figure 5 shows the typical cracking appearance in the test region of specimen C0 at starting of the cracking. The horizontal cracks were followed by vertical cracks throughout the length of the column. Then, the vertical

cracks gradually increased and widened as the load increased up to the peak point. The maximum axial load, P_{max}, sustained by the specimen was 3,531 kN. After peak, the column experienced a reduction in strength because of part of the concrete section failing. Then, the concrete cover was spalled off completely around the concrete core. The failure mode of the concentric columns was brittle and more sudden and explosive. Generally, for similar concrete strengths, lightweight aggregate concrete was comparatively brittle than normal weight concrete (NWC) (Cui et al., 2012). No buckling or crushing of GFRP bars were observed during the test. The failure of the column after testing is shown in Figure 5.

3.1.2 Specimens C50 and C200

The behavior of test specimens C50 and C200 was significantly affected by the level of the applied eccentricity. The response was essentially linear-elastic for both columns up to development of the first crack. The failure mechanism of both columns was defined as compression-controlled due to concrete crushing. The first flexural cracks were observed in tension sides at around 81% (1543.1 kN) and 16% (70.2 kN) of the peak load for specimens C50 and C200 respectively. At this step, the concrete cover in compression side of both columns was visually free of cracks. The failure of both columns characterized with the formation of horizontal hairline cracks in compression side followed by vertical cracks, at an applied load approximately equivalent to 98% of the peak load. Failure of the specimen C50 and C200 occurred respectively at an axial load of 1,905 kN and 439 kN (Figure 5). No buckling or crushing of GFRP bars were observed during the test. The failure of the columns after testing is shown in figure 6b and 6c for compression side and in Figure 6 for tension side.

a) Specimen C0 Specimen C50 (compression side) c) Specimen C200 (Compression side)

Fig. 5 – Overview of the test specimens after failure

a) Specimen C50 b) Specimen C50

Fig. 6 - Overview of the test specimens after failure in tension side

3.2 Axial-Displacement Response

The axial load-displacement relationships of all specimens are compared in Figure 7. The axial displacement was measured with two linear potentiometers (LPOTs) mounted on the ram head. The load–deformation of the test columns consisted only of a relatively linear ascending segment up to peak load. A decrease in the initial axial stiffness was observed with the increase of the loading. The average stiffness for test column C0, C50, and C200 was 583 kN/mm, 271 kN/mm and 26.5 kN/mm, respectively, up until the peak load level. This represents a decrease of the initial stiffness of 53.5% and 95.5% for columns C50 and C200, respectively. The axial displacement has increased with the increase of the eccentricity up to peak load. After this stage, a semi-linear ascending branch was developed to the peak load. This branch was characterized by a gradual loss of initial stiffness, mainly due to microcrack propagation on the compression side (for columns C0, C50 and C200) and flexural-tension cracks (for columns C50 and C200). After the peak load, the maximum capacity of the columns was reached, and the load was decreased or was constant with the increase of the axial load. The response of the load-axial displacement after the peak load was distinctively ductile due to the high ultimate strains of the GFRP bars and spirals. At the peak, the axial displacements for the columns C0, C50 and C200 were 6.4 mm, 7.4 mm and 16.4 mm.

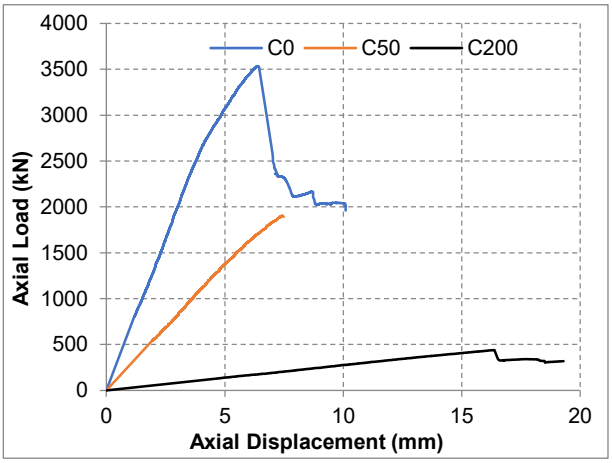

Fig. 5 - Load Axial-Displacement curves

3.3 Interaction Diagram

Figure 8 shows the failure points (peak loads) compared with the P-M diagram of GFRP concrete columns according to the procedure developed by (Zadeh et Nanni, 2013) that neglected the contribution of GFRP bars in compression. It can be observed that the failure point exhibits the characteristic “knee” shape found with steel RC columns in which the moment resistance increases as the axial load decreases until the inflection point is reached. However, the test results gave an upper bound for columns C0 and C200, which means that the predicted results were on the safe side.

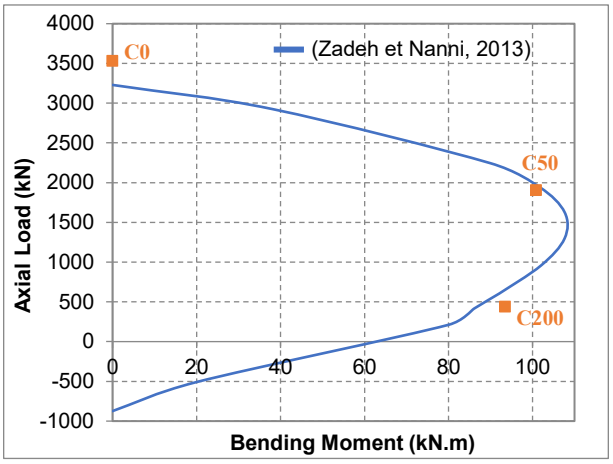

Fig. 8- Interaction Diagram for the GFRP-LWSCC columns

4. CONCLUSIONS

Full-scale circular lightweight self-consolidating concrete (LWSCC) columns reinforced with GFRP bars and spirals were tested under pure axial load and eccentricities, to investigate their behaviour and load capacities. The test parameter was the eccentricity-to-diameter ratio.

- The use of longitudinal GFRP bars is not detrimental to the performance of LWSCC RC columns.
- The failure process of GFRP LWSCC columns was similar to GFRP normal weight concrete columns.
- Compression failure due to concrete crushing controlled the ultimate capacity of the specimens tested under concentric. Flexural-tension and compression failure controlled the ultimate capacity of the specimens tested under eccentricity e/D of 16.4% and 65.7%.
- The axial displacement increased with the increase of the eccentricity up to peak load. The initial stiffness decreased by 53.5% and 95.5% for columns C50 and C200 compared to column C0.
- The interaction diagram for the tested GFRP RC columns showed the characteristic “knee” shape found with conventional steel RC columns.

5. ACKNOWLEDGMENTS

This research was conducted with funding from the Tier 1 Canada Research Chair in Advanced Composite Materials for Civil Structures, the Natural Sciences and Engineering Research Council of Canada, the Fonds de la recherche du Québec en nature et technologies (FQR-NT), and the Canadian Foundation for Innovation (FCI), and for the technical help provided by the staff of the structural lab of the Department of Civil Engineering at the University of Sherbrooke. The authors would like to express their special thanks and gratitude to Northeast Solite Corporation for their generosity. Their donation of Solite® aggregate was instrumental to the success of the research project.

6. REFERENCES

ACI Committee 213 (2014) Guide for Structural Lightweight-Aggregate Concrete (ACI 213R-14) (American Concrete Institute.). Farmington Hills, MI, USA : ACI.

ASTM C150 / C150M-18 (2019) Specification for Portland Cement (ASTM C150 / C150M-18). West Conshohocken : ASTM International.

ASTM C330/C330M-17a (2017) Standard Specification for Lightweight Aggregates for Structural Concrete (ASTM C330/C330M-17a). ASTM International, West Conshohocken, PA.

ASTM C567/C567M (2014) Standard Test Method for Determining Density of Structural Lightweight Concrete (ASTM C567/C567M-14). West Conshohocken, PA, 2014.

Benmokrane, B., El-Salakawy, E., El-Gamal, S. et Goulet, S. (2007) Construction and Testing of an Innovative Concrete Bridge Deck Totally Reinforced with Glass FRP Bars: Val-Alain Bridge on Highway 20 East. Journal of Bridge Engineering, vol. 12, n°5, p. 632-645.

CAN/CSA A23.3 (2014) Design of concrete structures. CSA Group.

Chandra, S. et Berntsson, L. (2002) Lightweight Aggregate Concrete: Science, Technology and Applications (1 edition.). William Andrew.

Comité euro-international du béton., Short, A. et Fédération internationale de la précontrainte. (1977) Lightweight aggregate concrete : CEB/FIP manual of design and technology. Lancaster, Eng.; New York : Construction Press.

Cui, H. Z., Lo, T. Y., Memon, S. A. et Xu, W. (2012) Effect of lightweight aggregates on the mechanical properties and brittleness of lightweight aggregate concrete. Construction and Building Materials, vol. 35, p. 149-158.

Hadhood Abdeldayem, Mohamed Hamdy M. et Benmokrane Brahim (2017) Experimental Study of Circular High-Strength Concrete Columns Reinforced with GFRP Bars and Spirals under Concentric and Eccentric Loading. Journal of Composites for Construction, vol. 21, n°2, p. 04016078.

Harmon, K. S. (2007) Engineering properties of structural lightweight concrete. Carolina Stalite Company.

International Congress on Lightweight Concrete, Brooks, A. E., Concrete Society, Cement and Concrete Association et Comité européen du béton (dir.) (1968) Proceedings of the First International Congress on Lightweight Concrete, London, May 1968; London : Cement and Concrete Association.

Mousa, A., Mahgoub, M. et Hussein, M. (2018) Lightweight concrete in America: presence and challenges. Sustainable Production and Consumption, vol. 15, p. 131-144.

Moy, S. (2013) Advanced fiber-reinforced polymer (FRP) composites for civil engineering applications. *In* N. Uddin (dir.), Developments in Fiber-Reinforced Polymer (FRP) Composites for Civil Engineering, Woodhead Publishing Series in Civil and Structural Engineering (p. 177-204). Woodhead Publishing.

Papanicolaou, C. et Kaffetzakis, M. (2011) Lightweight Aggregate Self-Compacting Concrete: State-of-the-Art & Pumice Application. Journal of Advanced Concrete Technology, vol. 9, p. 15-29.

Rabbat, B. G., Daniel, J. I., Weinmann, T. L. et Hanson, N. W. (1986) Seismic Behavior of Lightweight and Normal Weight Concrete Columns. Journal Proceedings, vol. 83, n°1, p. 69-79.

Real, S., Gomes, M. G., Moret Rodrigues, A. et Bogas, J. A. (2016) Contribution of structural lightweight aggregate concrete to the reduction of thermal bridging effect in buildings. Construction and Building Materials, vol. 121, p. 460-470.

Zadeh, H. J. et Nanni, A. (2013) Design of RC Columns Using Glass FRP Reinforcement. Journal of Composites for Construction, vol. 17, n°3, p. 294-304.